JOURNAL OF GEOPHYSICAL RESEARCH, VOL. 113, E10004, doi:10.1029/2007JE003032, 2008

Distribution and escape of molecular hydrogen in Titan's thermosphere and exosphere

J. Cui,[1,2] R. V. Yelle,[1] and K. Volk[1]

Received 30 October 2007; revised 24 May 2008; accepted 4 June 2008; published 7 October 2008.

[1] We present an in-depth study of the distribution and escape of molecular hydrogen (H_2) on Titan, based on the global average H_2 distribution at altitudes between 1000 and 6000 km, extracted from a large sample of Cassini/Ion and Neutral Mass Spectrometer (INMS) measurements. Below Titan's exobase, the observed H_2 distribution can be described by an isothermal diffusion model, with a most probable flux of $(1.37 \pm 0.01) \times 10^{10}$ cm^{-2} s^{-1}, referred to the surface. This is a factor of $\sim$3 higher than the Jeans flux of 4.5×10^9 cm^{-2} s^{-1}, corresponding to a temperature of 152.5 ± 1.7 K, derived from the background N_2 distribution. The H_2 distribution in Titan's exosphere is modeled with a collisionless approach, with a most probable exobase temperature of 151.2 ± 2.2 K. Kinetic model calculations in the 13-moment approximation indicate a modest temperature decrement of several kelvin for H_2, as a consequence of the local energy balance between heating/cooling through thermal conduction, viscosity, neutral collision, and adiabatic outflow. The variation of the total energy flux defines an exobase level of $\sim$1600 km, where the perturbation of the Maxwellian velocity distribution function, driven primarily by the heat flow, becomes strong enough to raise the H_2 escape flux considerably higher than the Jeans value. Nonthermal processes may not be required to interpret the H_2 escape on Titan. In a more general context, we suggest that the widely used Jeans formula may significantly underestimate the actual thermal escape flux and that a gas kinetic model in the 13-moment approximation provides a better description of thermal escape in planetary atmospheres.

Citation: Cui, J., R. V. Yelle, and K. Volk (2008), Distribution and escape of molecular hydrogen in Titan's thermosphere and exosphere, *J. Geophys. Res.*, *113*, E10004, doi:10.1029/2007JE003032.

1. Introduction

[2] Titan has a thick and extended atmosphere, which consists of over 95% molecular nitrogen (N_2), with methane (CH_4), molecular hydrogen (H_2) and other minor species making up the rest. The first in situ measurements of the densities of various species in Titan's upper atmosphere have been made by the Ion and Neutral Mass Spectrometer (INMS) on the Cassini orbiter during its close Titan flybys [*Waite et al.*, 2004]. In this paper we present our analysis of the vertical distribution of H_2 throughout Titan's thermosphere and exosphere, in a global average sense.

[3] In Titan's collision-dominated thermosphere, the production of hydrogen neutrals is significant below an altitude of $\sim$1000 km, mainly through the photodissociation of CH_4 and C_2H_2 [*Lebonnois et al.*, 2003]. Between this level and Titan's exobase at an altitude of $\sim$1500 km (defined traditionally as the level where the scale height of the atmospheric gas is equal to the mean free path of neutral collisions), the distribution of H_2 is usually described by a diffusion model [*Bertaux and Kockarts*, 1983; *Yelle et al.*, 2006]. In Titan's exosphere, the collisions between constituents are so rare that the problem becomes essentially one within the domain of the kinetic theory of free-streaming particles under the influence of Titan's gravity [*Fahr and Shizgal*, 1983]. The traditional exospheric model is based on a simple collisionless approach first proposed by *Öpik and Singer* [1961] and *Chamberlain* [1963], in an attempt to investigate the structure of the terrestrial exosphere. In such a model, the velocity distribution above the exobase is assumed to be a truncated Maxwellian, and particle densities can be directly calculated by integrating over the appropriate regions of the momentum space. Other choices of the velocity distribution at the exobase have also been investigated, such as the analytic power law and the κ distribution [e.g., *De La Haye et al.*, 2007].

[4] The escape of H_2 on Titan has been suggested to be mostly thermal and limited by diffusion [*Hunten*, 1973; *Bertaux and Kockarts*, 1983]. Conventionally, the thermal escape flux in planetary atmospheres is given by the Jeans formula. However, *Yelle et al.* [2006] observed an escape flux significantly larger than the Jeans value, through an analysis of the H_2 distribution in Titan's thermosphere. The Yelle et al. analysis is based on the data acquired during the first close encounter of Cassini with Titan (known in project

[1] Lunar and Planetary Laboratory, University of Arizona, Tucson, Arizona, USA.
[2] Department of Astronomy and Steward Observatory, University of Arizona, Tucson, Arizona, USA.

0148-0227/08/2007JE003032$09.00

Table 1. Summary of the Trajectory Geometry at C/A for All Titan Flybys Used in This Study

Flyby	Date	Alt (km)	LST (h:min)	SZA (deg)	Latitude (deg)	Longitude (deg)	F10.7 ($\frac{10^{-19}\text{erg}}{\text{cm}^2\ \text{s Hz}}$)
T5	16 Apr 2005	1027	23:17	128	74	89	83
T16	22 Jul 2006	950	17:21	105	85	45	72
T17	7 Sep 2006	1000	10:30	44	23	−56	87
T18	23 Sep 2006	962	14:25	90	71	3.0	70
T19	9 Oct 2006	980	14:20	81	61	2.6	75
T21	12 Dec 2006	1000	20:20	125	43	95	102
T23	13 Jan 2007	1000	14:02	53	31	2.1	81
T25	22 Feb 2007	1000	00:35	161	30	−16	76
T26	10 Mar 2007	981	01:45	150	32	2.1	71
T27	25 Mar 2007	1010	01:43	144	41	2.1	74
T28	10 Apr 2007	991	01:40	137	50	2.0	69
T29	26 Apr 2007	981	01:36	130	59	1.6	81
T30	12 May 2007	960	01:32	122	69	1.2	71
T32	13 Jun 2007	965	01:18	107	85	−1.2	71

parlance as TA). An updated investigation of the H_2 escape is necessary with the current more extensive Cassini/INMS data set.

[5] In this paper, we present our analysis of the H_2 distribution in Titan's thermosphere and exosphere. The global average H_2 density profile is obtained from a sample of INMS in situ measurements based on 14 low-altitude encounters of Cassini with Titan. The horizontal/diurnal variations of the H_2 distribution based on the same sample will be investigated in follow-up studies.

[6] The structure of this paper is as follows. We introduce the basic observations and describe data reductions in section 2. Simple one-dimensional models are presented in section 3, to describe the H_2 distribution at altitudes between 1000 and 6000 km. Regions below and above Titan's exobase are treated separately with different approaches. In section 4, we describe possible modifications of the simple exospheric model, considering in detail loss processes for H_2 and the energy balance in the transition region between the thermosphere and exosphere. Section 5 is devoted to understanding the escape of H_2 on Titan, in which we adopt a non-Maxwellian velocity distribution in the 13-moment approximation to calculate the thermal escape flux. Finally, discussion and conclusions are given in section 6.

2. Observations and Data Reductions

2.1. Observations

[7] Our investigation of Titan's thermosphere and exosphere relies exclusively on the observations made in the closed source neutral (CSN) mode, which is specifically designed to optimize interpretation of neutral species detected in the atmosphere of Titan or other INMS targets [*Waite et al.*, 2004]. In this mode, the inflowing gas particles enter the orifice of a spherical antechamber and thermally accommodate to the wall temperature before reaching the ionization region, the switching lens and the quadrupole mass analyzer. An enhancement in the signal-to-noise ratio of the sampled neutral species is accomplished by limiting the conductance from the antechamber to the ionization region, while maintaining high conductance through the entrance aperture [*Waite et al.*, 2004]. The geometric field of view of the CSN mode is as wide as 2π sr, and the angular response varies as the cosine of the angle between the INMS axis and the spacecraft velocity [*Waite et al.*, 2004].

[8] The INMS data consist of a sequence of counts in mass channels 1–8 and 12–99 amu. The H_2 densities in the ambient atmosphere are determined from counts in channel 2, which are typically sampled with a time resolution of 0.9 s, corresponding to a spatial resolution of 5.4 km along the spacecraft trajectory. In the 4 year length of the prime Cassini mission, there will be 44 close Titan flybys. Our work is based on 14 of them, known in project parlance as T5, T16, T17, T18, T19, T21, T23, T25, T26, T27, T28, T29, T30, and T32. The details of the encounter geometry for these flybys at closest approach (C/A) are summarized in Table 1, which shows that our sample preferentially selects measurements made over Titan's northern hemisphere, during nighttime, and at solar minimum conditions [see also *Müller-Wodarg et al.*, 2008].

2.2. Extraction of the H_2 Density Profile

[9] The counts in mass channel 2 are mainly contributed by H_2 molecules, with minor contributions from hydrocarbon species (CH_4, C_2H_2, etc.) ignored. Only inbound data are included in our analysis. This is because the INMS chamber walls have a certain probability to adsorb molecules entering the instrument orifice, which may further undergo complicated wall chemistry before being released with a time delay [*Vuitton et al.*, 2008]. Such a wall effect mainly takes place near C/A when the density in the ambient atmosphere is high, and primarily contaminates the outbound counts. In Figure 1, we compare the inbound and outbound H_2 density profiles averaged over all flybys in our sample (see below for the details on extracting the H_2 density profile from the raw measurements). The outbound H_2 densities are systematically higher than the inbound densities, with the deviation increasing at high altitudes. This is an indication of the importance of wall effect since other effects such as horizontal/diurnal variations should be smoothed by averaging. A more detailed discussion of the wall effects, including both the simple adsorption/desorption processes and the more complicated heterogeneous surface chemistry on the chamber walls, will be presented elsewhere (J. Cui et al., Analysis of Titan's neutral upper atmosphere from Cassini Ion Neutral Mass

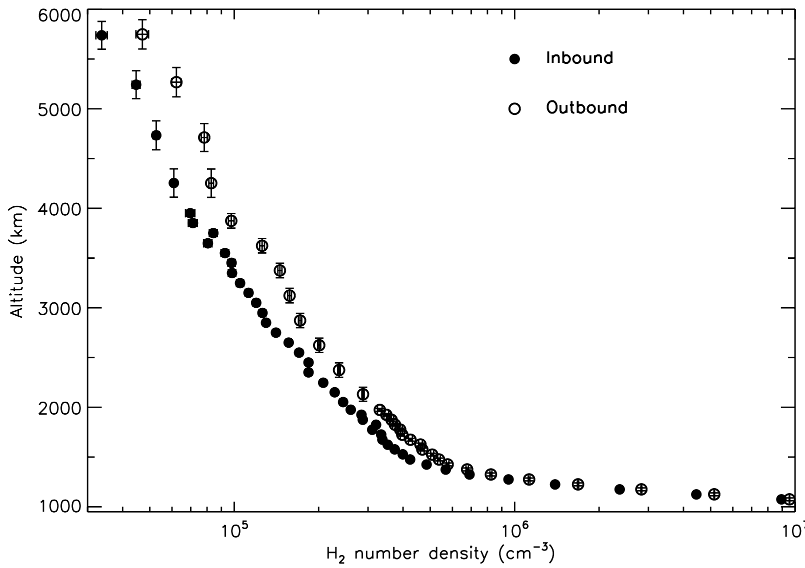

Figure 1. The global average H_2 distribution with $\pm 1\sigma$ uncertainties, in Titan's thermosphere and exosphere, as a function of altitude. The solid circles are for inbound densities, and the open circles for outbound. These density profiles are obtained by averaging INMS measurements from 14 close Titan flybys. Comparison between the average inbound and outbound H_2 profiles indicates that the wall chemistry effect is important for H_2. Our analysis relies exclusively on the inbound data.

Spectrometer measurements, manuscript in preparation, 2008).

[10] Corrections for thruster firings are required before the counts in channel 2 can be converted to H_2 densities [*Yelle et al.*, 2006]. The Cassini spacecraft thrusters operate with hydrazine (N_2H_4), with H_2 being a significant component of the thruster effluent. This effect is usually viewed as large excursions from the expected counts in channel 2, interspersed in the altitude range over which measurements were made. In most cases, contamination by thruster firings is serious near C/A when thrusters fire frequently to offset the torque on the spacecraft due to atmospheric drag [*Yelle et al.*, 2006]. Regions thought to be contaminated by thruster firings are identified by correlating with accumulated thruster operation time, accompanied by eyeball checking [*Yelle et al.*, 2006]. These regions are rejected from our analysis below.

[11] The counts in channel 2 tend to a constant level at very high altitudes above ~8000 km as a result of residual H_2 gas present in the INMS chamber. This effect causes significant overestimates of the H_2 densities of the ambient atmosphere at high altitudes if not properly removed. For each flyby, we use the inbound INMS data above an altitude of 10,000 km to evaluate the mean background signal in channel 2, assuming it is constant for any individual flyby. For the inbound pass of T25, the INMS measurements do not extend to altitudes above ~6000 km, and the background count rate averaged over all the other flybys is adopted. The mean background count rate varies from flyby to flyby, ranging between 70 and 240 counts s^{-1}.

[12] With thruster firings removed and background subtracted, counts in channel 2 are converted to H_2 number densities with a pre-flight laboratory calibration sensitivity of 3.526×10^{-4} counts $(cm^{-3}\ s)^{-1}$ [*Waite et al.*, 2004]. Since the preflight sensitivities were obtained for mixtures of reference gases with their isotopes, it is necessary to separate the contributions from H_2 and HD. The procedure used to correct for isotopic ratios will be presented elsewhere (Cui et al., manuscript in preparation, 2008).

[13] The conversion of INMS counts to densities of the ambient gas depends on the ram enhancement factor, which is a function of molecular mass, the angle of attack, and the spacecraft velocity relative to Titan [*Waite et al.*, 2004]. The conversion from channel 2 counts, C_2, to H_2 densities, n is

$$n = \frac{C_2}{(3.526 \times 10^{-4}) \times (0.031) \times \Re_{H2}}\ cm^{-3}, \qquad (1)$$

where 3.526×10^{-4} counts $(cm^{-3}\ s)^{-1}$ is the sensitivity, 0.031 s the integration time, and $\Re_{H2}$ the dimensionless ram enhancement factor. For the passes considered here, the INMS is pointed in the ram direction near C/A, allowing accurate density determination of the ambient gas. To improve the statistical significance of our analysis, we only include measurements with ram enhancement factors $\Re_{H2} \geq 5$, corresponding to ram angles $\leq 68°$ for a typical spacecraft velocity of 6 km s^{-1}. Response decreases significantly with increasing ram angle. For ram angles $\geq 90°$, the spacecraft configuration prevents the recording of any useful data of the ambient gas.

[14] To obtain the average H_2 distribution, the raw inbound measurements are binned by 50 km below an altitude of 2000 km, binned by 100 km between 2000 and 4000 km, and binned by 500 km above 4000 km. Such a profile is shown by the solid circles in Figure 1. Vertical error bars in Figure 1 represent the standard deviation of altitude for each bin. Horizontal error bars reflect uncertainties due to counting statistics, not necessarily associated with any horizontal/diurnal variations. The open circles in Figure 1 correspond to the average outbound H_2 profile

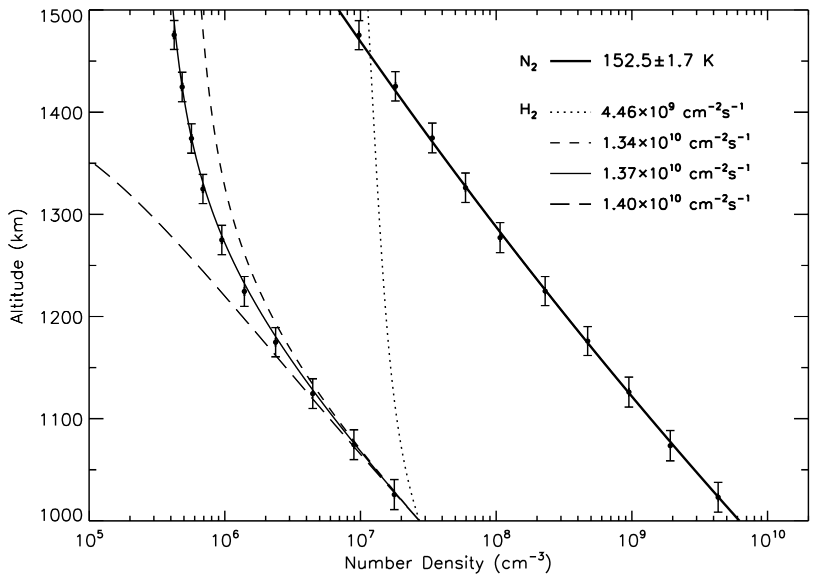

Figure 2. The average profiles of N_2 and H_2, with $\pm 1\sigma$ uncertainties, below Titan's exobase. The best fit barometric relation for the N_2 distribution is given by the thick solid line, with a most probable thermospheric temperature of (152.5 ± 1.7) K. For H_2, different curves correspond to different choices of the H_2 flux, with the solid line calculated with the most probable flux of $(1.37 \pm 0.01) \times 10^{10}$ cm^{-2} s^{-1}. The dotted line corresponds to the case with a Jeans flux of 4.46×10^9 cm^{-2} s^{-1}, which significantly deviates from the INMS data. All flux values are referred to Titan's surface, and the H_2 temperature is fixed as 152.5 K in all models.

determined in the same manner, which is contaminated by the wall effect (see above).

2.3. N_2 Density Profile and Barometric Fitting

[15] The determination of an average N_2 density profile is necessary for deriving the physical conditions of the background component. Here the contamination by thruster firings is unimportant because the N_2 density of the ambient atmosphere is much higher than that of the spacecraft effluent. For the detailed procedure of determining N_2 densities from counts in channels 14 and 28, see *Müller-Wodarg et al.* [2008]. The average N_2 distribution below an altitude of 2000 km is obtained by combining N_2 profiles from all flybys, binned by 50 km. Both inbound and outbound data of N_2 are included, since wall effects are not important for this species below 2000 km where the N_2 molecules in the ambient atmosphere are much more abundant than those formed on the chamber walls through surface chemistry.

[16] Such an average N_2 profile is shown in Figure 2, with $\pm 1\sigma$ uncertainties. Only the portion below 1500 km is presented. The thick solid line gives the best fit barometric relation of the observed N_2 distribution, with a most probable temperature of 152.5 ± 1.7 K. Also shown in Figure 2 is the average H_2 distribution in the same altitude range, as well as several model profiles calculated from the diffusion equation (see section 3.1). For comparison, we notice that the analysis of the inbound Voyager 1 UV solar occultation data by *Vervack et al.* [2004] estimated a temperature of 153 ± 5 K. *Yelle et al.* [2006] determined a similar temperature of 149 ± 3 K based on the INMS data acquired during the TA flyby. These previous determinations are in agreement with our value of ~153 K, which is also consistent with the empirical two-dimensional temperature distribution given by *Müller-Wodarg et al.* [2008], derived on the basis of a nearly identical INMS sample but with a different approach.

3. Preliminary Models of H_2 Distribution

3.1. H_2 Distribution in Titan's Thermosphere

[17] The H_2 distribution in Titan's collision-dominated thermosphere is usually modeled as a minor species (H_2) diffusing through a stationary background gas (N_2), following the formulation of *Chapman and Cowling* [1970]. This is similar to the 5-moment approximation to the Boltzmann momentum transport equation [*Schunk and Nagy*, 2000], with the additional assumption that the two interacting species have the same temperature. Adopting a constant H_2 temperature of 152.5 K based on the barometric fitting of the N_2 distribution (see section 2.3), the H_2 distribution is then described by the diffusion equation as

$$F_s\left(\frac{R}{r}\right)^2 = -Dn\left(\frac{1}{n}\frac{dn}{dr} + \frac{mg}{kT_0}\right), \qquad (2)$$

where R is Titan's radius, k is the Boltzmann constant, m is the mass of H_2 molecules, g is the local gravity, F_s is the H_2 flux referred to the surface, n is the H_2 number density, D is the molecular diffusion coefficient for H_2-N_2 gas mixture adopted from *Mason and Marrero* [1970], and T_0 = 152.5 K is the N_2 (also H_2) temperature. In equation (2), we have implicitly used the condition of flux continuity, since photochemical production and/or loss of H_2 is negligible above ~1000 km [e.g., *Lebonnois et al.*, 2003]. Eddy diffusion is ignored here since the altitude range under consideration is well above Titan's homopause at ~850 km [*Wilson and Atreya*, 2004; *Yelle et al.*, 2008]. More specifically, the molecular diffusion coefficient is 2×10^9 cm^2 s^{-1} at the lower boundary of 1000 km, about a factor of 70 greater than the eddy diffusion coefficient of $\sim 3 \times 10^7$ cm^2 s^{-1} [*Yelle et al.*, 2008]. We also ignore the higher-order thermal diffusion process in equation (2), since the temperature gradient over the relevant altitude range is small, of order 1 K over ~500 km (see section 4.1). From the kinetic theory, the ratio of the molecular diffusion term to the thermal diffusion term is $\sim 5kT_0F/q$, where q is the heat flux, $F = F_s(R/r)^2$ is the local H_2 flux, and the hard sphere approximation is assumed [see *Schunk and Nagy*, 2000, equation (4.129b)]. Adopting the solution for heat flux presented in section 4.1, the molecular diffusion term is estimated to be a factor of 60 larger than the thermal diffusion term at 1000 km.

[18] We solve equation (2) with a fourth-order Runge-Kutta algorithm, with the boundary condition of $n = 2.7 \times 10^7$ cm^{-3} at 1000 km inferred from the INMS data. The variation of gravity with altitude has been taken into account. In equation (2), the H_2 flux referred to the surface, F_s, is treated as a free parameter. On the basis of a χ^2 goodness-of-fit test between 1000 and 1500 km, the most probable value of the H_2 flux is found to be $F_s = (1.37 \pm 0.01) \times 10^{10}$ cm^{-2} s^{-1}. In Figure 2 we show the model H_2 distribution calculated from equation (2) with different choices of F_s. Also shown in Figure 2 are the INMS data binned by 50 km. The solid line corresponds to the most probable value of $F_s = 1.37 \times 10^{10}$ cm^{-2} s^{-1}, whereas the dotted line corresponds to the Jeans flux of 4.46×10^9 cm^{-2} s^{-1}, calculated with an exobase temperature of 152.5 K. The most probable H_2 flux is about a factor of 3 higher than the Jeans value, implying an enhanced escape of H_2 on Titan. The interpretation of such a large H_2 escape flux will be discussed in section 5.

[19] Figure 2 shows that the diffusion model, assuming full thermal coupling between H_2 and N_2, provides a reasonable description of the observed H_2 distribution below ~1500 km. On the basis of a similar analysis of the Cassini/INMS data acquired during the TA flyby, *Yelle et al.* [2006] obtained an H_2 flux of $(1.2 \pm 0.2) \times 10^{10}$ cm^{-2} s^{-1} (referred to the surface), which is consistent with our result.

3.2. H_2 Distribution in Titan's Exosphere

[20] To model the H_2 distribution above Titan's exobase, we adopt a kinetic approach based on the solution of the collisionless Boltzmann equation [*Chamberlain and Hunten*, 1987]. Following the idea originally conceived by *Öpik and Singer* [1961] and *Chamberlain* [1963], any particle in the exosphere naturally falls into one of four categories based on orbital characteristics, i.e., ballistic, satellite, escaping, and incoming hyperbolic particles. At any given point in the exosphere, each of the above types occupies an isolated region in the momentum space. Ballistic and escaping particles intersect the exobase, with velocities either smaller or greater than the escape velocity. These two categories represent particles which are directly injected from the thermosphere. On the other hand, satellite particles have perigees above the exobase, and therefore have a purely exospheric origin. Because in any collisionless model, there is no mechanism to establish a steady population of satellite particles, this category is excluded from our calculations. The incoming hyperbolic particles, which obviously require an external origin, are also excluded.

[21] Assuming a Maxwellian velocity distribution function (VDF) at the exobase, Liouville's theorem implies that the VDF for H_2 molecules above this level is also Maxwellian, but truncated to include only regions in the momentum space occupied by either ballistic or escaping particles with trajectories intersecting the exobase. The H_2 densities in the exosphere can be determined by integrating over the Maxwellian VDF within the truncated regions. Analytical results for these integrations are given by *Chamberlain* [1963]. The model exospheric profile only depends on the density and temperature of H_2 at the exobase, which are treated as two free parameters in the model fitting. The most probable values of these parameters are found to be $n_{exo} = (4.34 \pm 0.02) \times 10^5$ cm^{-3} and $T_{exo} = 151.2 \pm 2.2$ K, where the exobase is placed at an altitude of 1500 km. Although the definition of the exobase level is itself subject to uncertainty, the results presented in this section are not sensitive to the exact choice, as a result of the large H_2 scale height (~1000 km near the exobase). However, in section 5.3 we show that a more realistic exobase height is ~1600 km, which has important implication on the derived thermal escape flux.

[22] The exospheric H_2 distribution calculated from such a collisionless model is shown in Figure 3, overplotted on the INMS data. Different profiles correspond to different choices of the exobase temperature, with the solid line representing the most probable value of 151.2 ± 2.2 K, consistent with the N_2 temperature of 152.5 K within 1σ. The dotted line shows the exospheric H_2 profile calculated from collisionless Monte Carlo simulations, taking into account Saturn's gravitational influence (see section 5.1 for details).

4. Thermal Effect and Loss Processes of H_2

[23] In section 3, we show that the simple collisionless model reasonably describes the observations of H_2 in Titan's exosphere. Here we investigate two physical mechanisms that may potentially modify the exospheric H_2 distribution: (1) the thermal disequilibrium between H_2 and N_2 caused by escape and (2) the external loss processes of H_2 above Titan's exobase. We will show below that neither of the mechanisms has a substantial influence on the H_2 distribution. However, taking into account the actual thermal structure may have important implications in interpreting the observed H_2 escape, which is discussed in section 5.3.

4.1. Temperature Decrement for H_2 Near Titan's Exobase

[24] Early observations of the terrestrial exosphere have shown a significant temperature decrement for atomic H, as large as ~100 K near the exobase [*Atreya et al.*, 1975]. To interpret this, *Fahr* [1976] has suggested that a correct description of the exospheric model must satisfy energy continuity, in addition to momentum and particle conservation. This condition requires that the energy loss due to

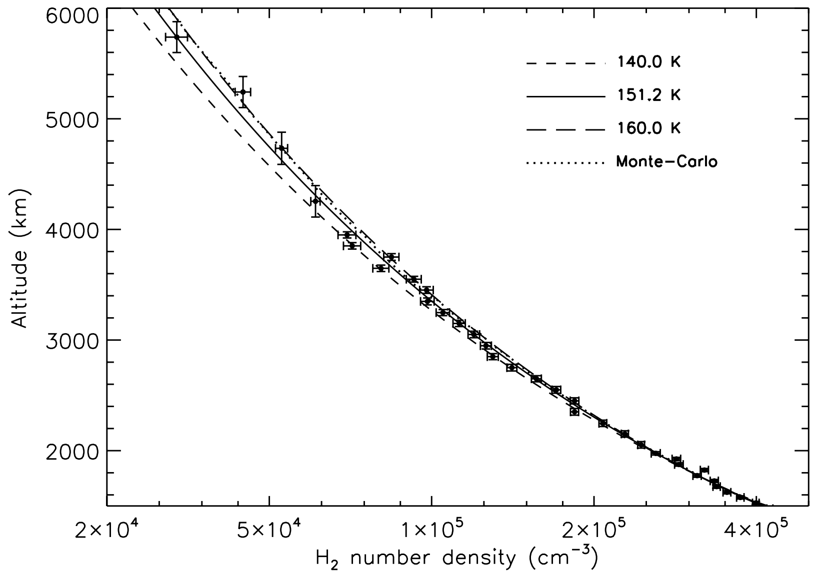

Figure 3. The H_2 density profiles calculated with the collisionless model, assuming a truncated Maxwellian VDF for exospheric particles. Different lines correspond to different choices of the exobase temperature, with the solid line representing the most probable value of 151.2 K. The dotted line shows the exospheric H_2 profile calculated from collisionless Monte Carlo simulations, including Saturn's gravitational influence. An exobase height of 1500 km is adopted. The models are overplotted on the INMS measurements averaged over 14 Titan flybys.

particle escape be balanced by an appropriate energy supply through thermal conduction, which is naturally associated with a temperature gradient for the escaping component [*Fahr*, 1976; *Fahr and Weidner*, 1977]. For Titan, such a thermal effect implies a temperature difference between the background N_2 gas at T_0 and the diffusing H_2 gas at $T < T_0$. However, this effect should be assessed quantitatively, such that the calculated temperature reduction for H_2 does not contradict the INMS observations. In section 3, we have already seen that the H_2 gas is approximately in thermal equilibrium with N_2, as indicated by the closeness of their temperatures near the exobase.

[25] To investigate the thermal effect, we adopt a 13-moment approximation to the kinetic theory, which has been extensively used in modeling the terrestrial polar wind [*Lemaire et al.*, 2007; *Tam et al.*, 2007]. In such an approximation, the Boltzmann energy transport equation is given by *Schunk and Nagy* [2000] as

$$\frac{1}{r^2}\frac{d}{dr}\left(r^2\Phi_{\mathrm{E}}\right) = 3k\frac{m}{m_0}n\nu(T_0 - T) - mn\nu\left(\frac{F}{n}\right)^2, \qquad (3)$$

where $F = F_s(R/r)^2$ is the local H_2 flux with F_s adopted as the most probable value derived from the diffusion equation (R is Titan's radius), m and m_0 are the molecular masses of H_2 and N_2, and T and T_0 are their temperatures of which the latter is fixed as 152.5 K. The quantity, ν in equation (3) is the H_2-N_2 neutral collision frequency, which is related to the diffusion coefficient, D, in equation (2) through $\nu D = kT/m$ [*Schunk and Nagy*, 2000]. Φ_{E} represents the local energy flux, given as

$$\Phi_{\mathrm{E}} = mF\left(c_{\mathrm{p}}T + \frac{u^2}{2} - \frac{GM}{r}\right) - \kappa\frac{dT}{dr} - \frac{4}{3}\eta u\left(\frac{du}{dr} - \frac{u}{r}\right), \qquad (4)$$

where $c_p = (5/2)(k/m) = 1.03 \times 10^8$ ergs K^{-1} g^{-1} is the specific heat of H_2 at constant pressure, G is the gravitational constant, M is Titan's mass, $u = F/n$ is the drift velocity of H_2, κ and η are the thermal conductivity and the viscosity coefficient. We adopt $\kappa = 1.1 \times 10^4$ ergs cm^{-1} K^{-1} and $\eta = 5.5 \times 10^{-5}$ g cm^{-1} s^{-1} for the appropriate temperature [*Rowley et al.*, 2003]. The first term on the right-hand side of equation (4) corresponds to the intrinsic energy flux of H_2, with contributions from the internal energy, the bulk kinetic energy and the gravitational energy added together. The other two terms represent the energy transfer through thermal conduction and viscosity. The derivation of equation (4) is provided in the appendix. Equation (3) characterizes the local energy balance of H_2 on Titan. The equation includes the effect of energy transfer from N_2 to H_2 through neutral collisions given by the right-hand side (the meanings of the two terms will be addressed below). The effects of thermal conduction, viscosity, as well as adiabatic cooling due to H_2 outflow are included in the divergence term on the left-hand side of equation (3).

[26] We solve equation (3) for the H_2 thermal structure at altitudes between 1000 and 2500 km. Boundary conditions have to be specified to complete the problem, including one for T and one for dT/dr. We assume that the H_2 and N_2 gases are in thermal equilibrium at the lower boundary, i.e., $T = T_0 = 152.5$ K at 1000 km. The boundary condition for the temperature gradient is determined by the requirement of energy continuity at the upper boundary, which can be expressed as

$$\Phi_{\mathrm{E}} = 2\pi\int_{v_{\mathrm{esc}}}^{\infty} v^2 dv \int_0^1 d\cos\theta f(v,\theta)\left(\frac{1}{2}mv^2 - \frac{GMm}{r}\right)v\cos\theta, \quad (5)$$

where v_{esc} is the escape velocity at the upper boundary and $f(v, \theta)$ is the VDF for H_2 molecules, which is assumed to be

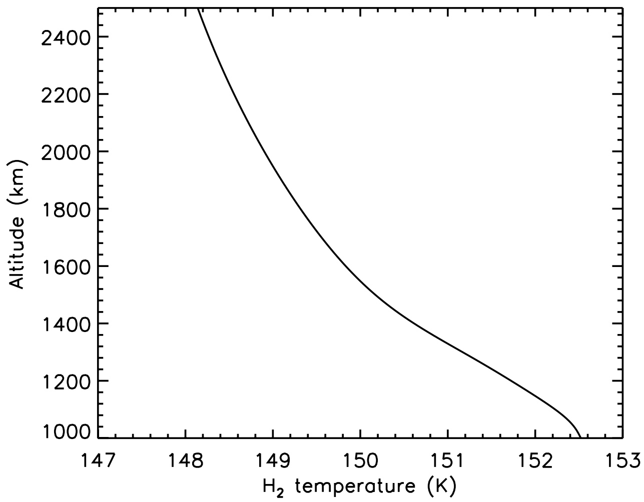

Figure 4. The thermal structure for the diffusing H_2 component on Titan, calculated from equation (3) and satisfying energy flux continuity at the upper boundary. The model predicts a modest temperature decrement of $\sim$2 K for H_2 from the lower boundary to the exobase.

independent of the azimuthal angle but allows for dependence on the polar angle. The simplest scheme is to adopt the drifting Maxwellian distribution. However, the realistic VDF for H_2 molecules at the upper boundary is not strictly Maxwellian. To correct for this, we adopt the VDF for H_2 molecules in the 13-moment approximation. The appropriate form of such a distribution function will be presented in section 5.3. Here, we emphasize that both the drifting Maxwellian and the 13-moment VDF depend on the values of some unknown parameters at the upper boundary (e.g., temperature and drift velocity). This requires that equations (3), (4), and (5) be solved in an iterative manner to ensure self-consistency.

[27] Figure 4 presents the calculated thermal structure for the diffusing H_2 component, which predicts an H_2 temperature of 150.1 K at 1500 km, or a temperature decrement of 2.4 K. This is consistent with the INMS observations, which give a most probable exobase H_2 temperature of 151.2 K based on the collisionless Chamberlain approach (see section 3.2). However, the predicted thermal effect is too small to get firm supports from the data, since the uncertainties in the temperature determination are considerably larger. A similar calculation in the 13-moment approximation has been carried out by *Boqueho and Blelly* [2005] on various neutral components in the Martian atmosphere, which shows that the thermal structure of relatively light species such as O present a modest temperature decrement of order 1 K near the exobase (see Boqueho and Blelly's Figure 8), comparable to our results.

[28] In Figure 5 we show the relative magnitudes of various terms in equation (3) which represent the energy gain/loss rates associated with heat conduction (solid), viscosity (short-dashed), adiabatic outflow (dotted), as well as H_2-N_2 neutral collisions (long-dashed). Heating and cooling terms are shown in the left panel and right panel, respectively. First, we notice that though the background N_2 gas is warmer than H_2, neutral collisions between the two components do not necessarily mean 'heating'. The energy transfer through collisions is represented by the right-hand side of equation (3), which consists of two terms. The first term characterizes the energy transfer due to random motion of the colliding particles, which always acts to heat the H_2

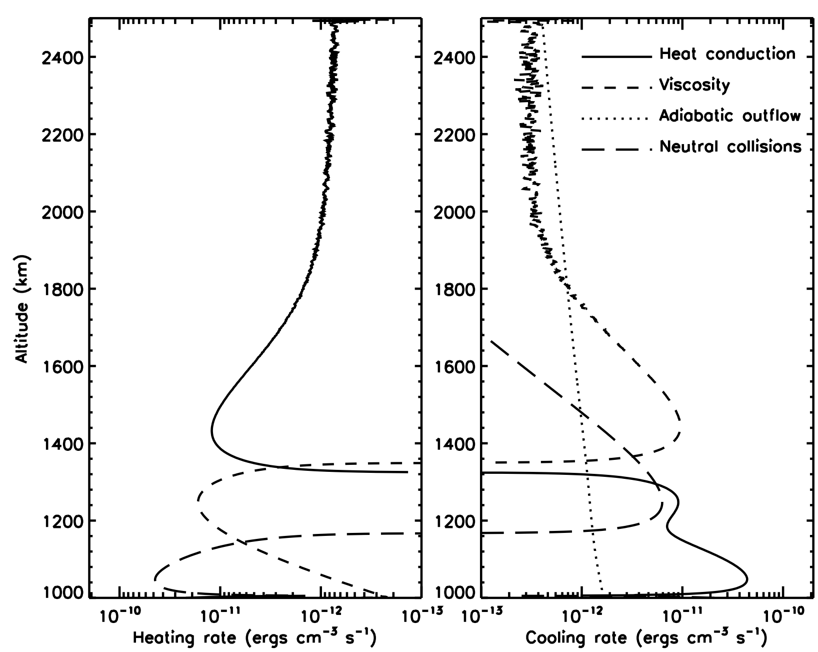

Figure 5. The relative magnitudes of various terms in the 13-moment energy equation (equation (3)). Different lines represent the energy gain/loss rates associated with different mechanisms, including thermal conduction (solid), viscosity (short-dashed), adiabatic outflow (dotted), and H_2-N_2 neutral collisions (long-dashed).

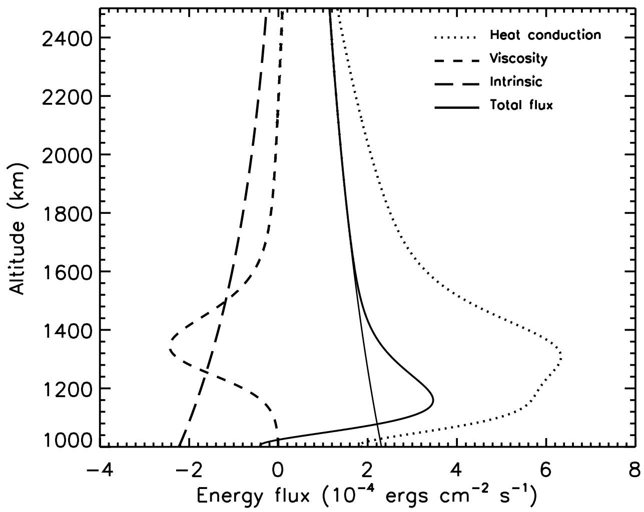

Figure 6. The relative magnitudes of various energy fluxes, including the conductive heat flux (dotted), the viscous energy flux (short-dashed), and the intrinsic energy flux (long-dashed) which combines the internal energy, the gravitational energy, as well as the bulk kinetic energy. The total energy flux is given by the thick solid line, which tends to follow the condition of energy flux continuity (given by the thin solid line) above ~1600 km.

gas. The second term shows that the bulk diffusive motion of H_2 through the stationary N_2 gas is decelerated by their mutual interactions, acting as a cooling mechanism. Whether the net effect of neutral collisions is heating or cooling depends on the relative magnitudes of these two mechanisms. According to our model calculations, the effect of neutral collisions between H_2 and N_2 is heating below ~1160 km and cooling above. The effect of thermal conduction can be either heating (above ~1320 km) or cooling (below ~1320 km), which is always an important energy term in the local energy budget, except near 1300 km. The effect of viscosity also switches between heating and cooling (at an altitude of ~1350 km). Finally, adiabatic outflow is always a cooling mechanism, and is important above ~1800 km. Figure 5 shows that well below the exobase, the energy gain through neutral collisions is primarily balanced by energy loss through thermal conduction. However, well above the exobase, the local energy budget is a balance between energy gain through thermal conduction and energy loss through both viscous dissipation and adiabatic outflow. In the transition region between the thermosphere and exosphere, the energy budget is more complicated and an individual energy term may switch between heating and cooling as mentioned above.

[29] The energy budget of H_2 implied in the 13-moment model is more complicated than that described in early works [*Fahr*, 1976; *Fahr and Weidner*, 1977], in which the thermal structure of the diffusing component was obtained by assuming equality between the escaping energy flux, Φ_{esc} and the conductive heat flux. This corresponds to a simplified case of the boundary condition given by equation (5), which ignores both the intrinsic and viscous energy fluxes. To examine the relative magnitudes of various energy fluxes, in Figure 6 we show different terms from the right-hand side of equation (4) as a function of altitude. The dotted, short-dashed and long-dashed lines represent the conductive heat flux, the viscous energy flux, and the intrinsic energy flux, respectively. The total energy flux is shown by the thick solid line in Figure 6, along with the condition of energy flux continuity (given by the thin solid line). Above ~1600 km, the total energy flux tends to scale as $1/r^2$, implying negligible effects of neutral collisions according to equation (3). Correspondingly, the exobase of Titan can be placed at ~1600 km based on Figure 6. At this altitude, the total downward energy flux counteracts roughly 50% of the upward conductive heat flux, indicating that the neglect of intrinsic and viscous energy fluxes in the early works is not justified here. The exobase height of ~1600 km implied by the variation of total energy flux is higher than the traditional choice of ~1400–1500 km estimated from a comparison between the atmospheric scale height and mean free path. The implication of this result on the thermal escape flux is discussed in section 5.3.

[30] Finally, we mention that although the thermal effect for H_2 on Titan is not significant, in terms of the absolute value of the temperature decrement, we will show in section 5.3 that the associated heat flux provides an important modification to the velocity distribution of H_2 molecules. In fact, the consequence of the non-Maxwellian VDF for the escape flux is so large that it may completely invalidates the Jeans formula.

4.2. External Loss of H_2 in Titan's Exosphere

[31] Titan's exosphere is subject to solar EUV radiation, and is, most of the time, within Saturn's magnetosphere. The exospheric distribution of H_2 on Titan may therefore be affected by its interactions with either solar photons or magnetospheric particles through external loss processes. These processes include photoionization and photodissociation, electron impact ionization, as well as charge transfer reactions with energetic protons/ions in the magnetosphere.

[32] Whether a particular loss process appreciably influences the exospheric H_2 distribution relies on a comparison between the corresponding loss timescale and the dynamical time of H_2 molecules spending above the exobase, following their own orbits. To investigate this, we draw a random sample of ~22,000 particles from the Maxwellian distribution with a temperature of 152.5 K. The trajectories of these particles, assumed to be injected from Titan's exobase in random upward directions, are calculated and averaged. For ballistic particles, the inferred mean dynamical time increases from 1×10^3 s (on ascending trajectories) and 9×10^3 s (on descending trajectories) at an altitude of 2000 km, to 7×10^3 s (ascending) and 5×10^4 s (descending) at 6000 km. The mean dynamical time for escaping particles varies from 5×10^2 s at 2000 km to 3×10^3 s at 6000 km. Averaged over all particle types and weighted by their number fractions, the total mean dynamical time is found to be 5×10^3 s at 2000 km and 2×10^4 s at 6000 km. Clearly, any external loss process is more efficient at depleting particles on ballistic trajectories, since the loss probability scales exponentially with the dynamical timescale (see equation (7)).

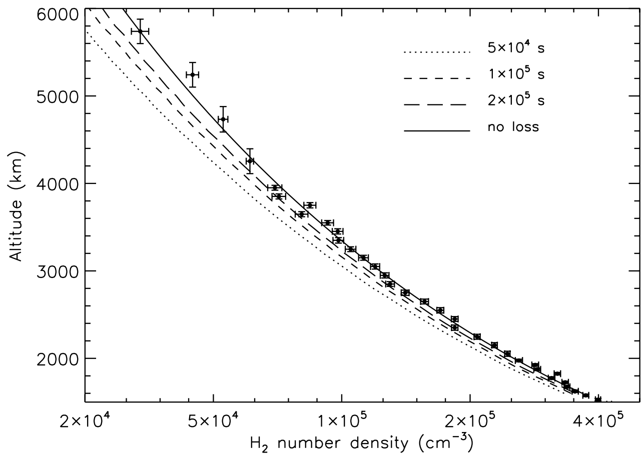

Figure 7. The model H_2 density profiles calculated with different values of the constant timescale for H_2 loss, assuming an exobase temperature of 152.5 K. The models are overplotted on the INMS data for comparison. The solid line corresponds to the case with no external loss mechanism.

[33] Assuming that a particular loss process is characterized by a constant timescale of $\tau_{\rm loss}$, the H_2 density distribution can be calculated by

$$n(r) = n_{\rm exo} e^{-(\lambda_{\rm exo}-\lambda)}\left[\zeta'_{\rm bal}(\lambda) + \zeta'_{\rm esc}(\lambda)\right], \quad (6)$$

where $\lambda = (GMm)/(kT_{\rm exo}r)$ and $\lambda_{\rm exo}$ is the value at the exobase with $r_{\rm exo}$ = 4075.5 km. For simplicity, we have implicitly assumed a Maxwellian velocity distribution and adopted $T = T_{\rm exo}$ = 152.5 K at all altitudes above the exobase. Taking into account the non-Maxwellian VDF as well as the actual thermal structure should not alter our results significantly. In equation (6), $\zeta'_{\rm bal}$ and $\zeta'_{\rm esc}$ are the partition functions for ballistic and escaping particles, which take into account the loss processes. Extending the formalism of *Chamberlain* [1963] to include loss processes, we can express the partition functions as

$$\zeta'_{\rm bal}(\lambda) = \frac{2}{\pi^{1/2}}\left[\int_0^{\xi_1} d\xi \int_0^{\chi_1} d\chi e^{-\xi^2-\chi-\frac{t(\lambda,\xi,\chi)}{\tau_{\rm loss}}} + \int_{\xi_1}^{\lambda^{1/2}} d\xi \int_0^{\chi_2} d\chi e^{-\xi^2-\chi-\frac{t(\lambda,\xi,\chi)}{\tau_{\rm loss}}}\right], \quad (7)$$

$$\zeta'_{\rm esc}(\lambda) = \frac{1}{\pi^{1/2}}\left[\int_{\xi_1}^{\lambda^{1/2}} d\xi \int_{\chi_2}^{\chi_1} d\chi e^{-\xi^2-\chi-\frac{t(\lambda,\xi,\chi)}{\tau_{\rm loss}}} + \int_{\lambda^{1/2}}^{\infty} d\xi \int_0^{\chi_1} d\chi e^{-\xi^2-\chi-\frac{t(\lambda,\xi,\chi)}{\tau_{\rm loss}}}\right], \quad (8)$$

where $t(\lambda, \xi, \chi)$ is the dynamical time required by a particle to travel from the exobase to a given point in the exosphere, following its own orbit. The integration limits in equations (7) and (8) are given by $\chi_1 = \lambda^2(\lambda_{\rm exo} - \lambda + \xi^2)/(\lambda_{\rm exo}^2 - \lambda^2)$, $\chi_2 = \lambda - \xi^2$, and $\xi_1 = \lambda(1 - \lambda/\lambda_{\rm exo})$ [*Chamberlain and Hunten*, 1987]. The exponential factor of $\exp[-t(\lambda, \xi, \chi)/\tau_{\rm loss}]$ represents the probability that an H_2 molecule survives the loss process under consideration. $t(\lambda, \xi, \chi)$ can be calculated by

$$t^+(\lambda,\xi,\chi) = \frac{GMm}{kT_{\rm exo}v_{\rm th}} \int_\lambda^{\lambda_{\rm exo}} \frac{d\lambda}{\lambda^2(\xi^2+\lambda)^{1/2}} \quad (9)$$

for $\xi > 0$ and

$$t^-(\lambda,\xi,\chi) = 2\frac{GMm}{kT_{\rm exo}v_{\rm th}} \int_{\lambda_{\rm exo}}^{\lambda_{\rm m}} \frac{d\lambda}{\lambda^2(\xi^2+\lambda)^{1/2}} - t^+(\lambda,\xi,\chi) \quad (10)$$

for $\xi < 0$, where $v_{\rm th} = (2kT_{\rm exo}/m)^{1/2}$ is the thermal velocity of H_2 at the exobase, and $\lambda_{\rm m}$ corresponds to the maximum radius reached by an H_2 molecule along its orbit (only for ballistic particles). Equations (9) and (10) correspond to the situations in which the H_2 molecule is on the ascending and descending portions of its trajectory, respectively. Escaping particles do not have descending trajectories, and should be excluded from equation (10).

[34] In Figure 7 we show the model H_2 profiles calculated from equations (6)–(10), overplotted on the INMS measurements. Different lines represent different choices of the constant loss timescale, $\tau_{\rm loss}$, with the solid one giving the reference case with no external H_2 loss. Figure 7 indicates that a loss timescale of order 10^5 s is required to have an appreciable effect on the observed exospheric H_2 distribution. We show below that all reasonable loss processes of H_2 have typical timescales much longer than $\sim 10^5$ s, therefore the exospheric distribution of H_2 molecules cannot be significantly modified by these loss processes.

4.2.1. Photoionization and Photodissociation

[35] H_2 molecules are ionized by solar EUV photons with energy above 15.4 eV. Assuming an exosphere that is optically thin to the solar EUV radiation, the photoionization timescale, $t_{\rm ion}$ can be calculated from

$$t_{\rm ion}^{-1} = \int \pi\tilde{F}_\odot(\tilde{\lambda})\tilde{\sigma}_{\rm ion}(\tilde{\lambda})d\tilde{\lambda}, \quad (11)$$

where $\tilde{\lambda}$ is the wavelength, $\tilde{\sigma}_{\rm ion}(\tilde{\lambda})$ is the photoionization cross section of H_2 molecules, and $\pi\tilde{F}_\odot(\tilde{\lambda})$ is the solar spectral irradiance. We adopt the analytic formulae for H_2 photoionization cross section from *Yan et al.* [1998], which combines experimental results at low energies and theoretical calculations at high energies. For the solar EUV irradiance, we adopt the sounding rocket measurements made on 3 November 1994, appropriate for solar minimum conditions during solar cycle 22 [*Woods et al.*, 1998]. The corresponding F10.7 cm flux is 86 at 1 AU, comparable with the average value of 77 for our INMS sample. With the solar irradiances scaled to the value at Titan, equation (11) gives $t_{\rm ion} = 8.8 \times 10^8$ s.

[36] H_2 molecules are also destroyed through dissociation by solar EUV photons at energies between the Lyman continuum and Lyα. Destruction of H_2 by photodissociation is accomplished through the Solomon process, i.e., upward transitions to electronic excited states followed by spontaneous decays to the vibrational continuum of the ground state [e.g., *Abgrall et al.*, 1992]. We adopt the parameters for individual transitions in the Lyman and Werner bands

Table 2. Characteristic Timescales

Process	t_{loss} (s)	Note
Photoionization	9×10^8	solar minimum
Photodissociation	7×10^8	solar minimum
Electron impact ionization	1×10^9	hot electrons
	3×10^8	cold electrons
Charge transfer	5×10^9	$H_2 + p \to H_2^+ + H$
	2×10^9	$H_2 + O^+ \to H_2^+ + O$
Dynamical timescale[a]	4×10^3	upward ballistic
	3×10^4	downward ballistic
	2×10^3	escaping

[a]Mean dynamical timescales required by particles with different orbital characteristics to reach an altitude of 4000 km, assuming they are injected in random upward directions and satisfy the Maxwellian VDF with a temperature of 152.5 K.

published by *Abgrall et al.* [1992] and the spontaneous radiative dissociation rate from *Abgrall et al.* [2000]. The photodissociation timescale, $t_{\rm dis}$ can then be expressed as

$$t_{\rm dis}^{-1} = 8.85 \times 10^{-6} \Sigma_{ij} \pi \tilde{F}_{\odot}\left(\tilde{\lambda}_{ij}\right) \tilde{f}_{ij} \tilde{P}_j \tilde{\lambda}_{ij}^2 \ {\rm s}^{-1}, \quad (12)$$

where i and j refer to the lower and upper state of an electronic transition, $\tilde{f}_{ij}$ and $\tilde{\lambda}_{ij}$ are the f value and central wavelength of the corresponding transition, $\tilde{P}_j$ is the probability that an H_2 molecule at the electronic excited state j spontaneously decays to the vibrational continuum of the ground state. Here $\pi\tilde{F}_{\odot}$ is in units of photons s^{-1} cm^{-2} Å^{-1}, and $\tilde{\lambda}_{ij}$ in units of Å. The summation is over all dipole-allowed transitions in the Lyman and Werner bands. In obtaining equation (12), we have also assumed a Doppler line profile, and the integrated results are independent of the adopted exobase temperature. From equation (12) we estimate an H_2 photodissociation timescale of $t_{\rm dis} = 7.2 \times 10^8$ s.

4.2.2. Interactions With Saturn's Magnetosphere

[37] Titan has a nonexistent or very weak intrinsic magnetic field, and its exosphere is, most of the time, directly subject to bombardment by energetic ions/protons and electrons in Saturn's corotating plasma. Here we investigate the interactions between Titan's exospheric H_2 molecules and Saturn's magnetosphere through the following processes:

$$H_2 + p \longrightarrow H_2^+ + H, \quad (13)$$

$$H_2 + O^+ \longrightarrow H_2^+ + O, \quad (14)$$

$$H_2 + e^* \longrightarrow H_2^+ + e + e^*, \quad (15)$$

where p is proton and e^* is energetic electron. Rather than integrating over the full energy distribution of the incident fluxes, we approximate the timescale, t_i for each of the above reactions by

$$t_i^{-1} \approx n_i \tilde{\sigma}_i(E_i) \left(\frac{2E_i}{m_i}\right)^{1/2}, \quad (16)$$

where i stands for either proton, electron, or singly ionized oxygen, n_i, E_i, and m_i are the density, energy, and particle mass of species i, and $\tilde{\sigma}_i(E_i)$ is the cross section for reaction between i and H_2 at incident energy E_i.

[38] To calculate t_i, we adopt results from the extended plasma model for Saturn, constructed on the basis of the data from Voyager 1 and 2 plasma (PLS) experiments [*Richardson and Sittler*, 1990; *Richardson*, 1995]. We use model parameters obtained at $L \approx 20$ to represent plasma conditions close to Titan's orbit around Saturn. For protons, we use $n_p = 0.1$ cm^{-3} and $E_p = 50$ eV; for O^+, we use $n_{O+} = 0.13$ cm^{-3} and $E_{O+} = 280$ eV [*Richardson*, 1995]. The electron energy distribution in Saturn's outer magnetosphere is characterized by a cold thermal component and a hot suprathermal component [*Sittler et al.*, 1983]. For hot electrons, we use $n_{e,\rm hot} = 0.019$ cm^{-3} and $E_{e,\rm hot} = 600$ eV [*Richardson*, 1995]. The cold thermal electron component is highly time variable, and the temperature variation is anti-correlated with the density variation [*Sittler et al.*, 1983]. Here we use values from Voyager 1 inbound measurements made at $L \approx 15$ (day 317, 10:29), with $n_{e,\rm cold} = 0.4$ cm^{-3} and $E_{e,\rm cold} = 21$ eV [*Sittler et al.*, 1983]. The cross sections for reactions (13)–(15) are adopted as $\tilde{\sigma}_p = 2.0 \times 10^{-16}$ cm^{-2} at an incident energy of 48 eV [*McClure*, 1966]; $\tilde{\sigma}_{O+} = 8.1 \times 10^{-16}$ cm^{-2} at 300 eV [*Nutt et al.*, 1979]; $\tilde{\sigma}_{e,\rm cold} = 3.3 \times 10^{-17}$ cm^{-2} at 21 eV and $\tilde{\sigma}_{e,\rm hot} = 3.6 \times 10^{-17}$ cm^{-2} at 600 eV [*Kim and Rudd*, 1994]. With these values, we estimate the characteristic timescales for reactions (13)–(15) as $t_p \approx 5.1 \times 10^9$ s, $t_{O+} \approx 1.6 \times 10^9$ s, $t_{e,\rm hot} \approx 1.0 \times 10^9$ s, and $t_{e,\rm cold} \approx 2.8 \times 10^8$ s.

[39] To summarize, we list all the relevant timescales in Table 2. Various external loss processes have characteristic timescales between 3×10^8 s and 5×10^9 s, which are much longer than the dynamical time of H_2 molecules above the exobase. This indicates that the exospheric distribution of H_2 on Titan is not significantly modified by these loss processes.

5. Escape of H_2 on Titan

[40] We have shown in section 4.1 that the H_2 escape flux inferred from the diffusion model is about a factor of 3 higher than the Jeans value, implying an enhanced escape of H_2 on Titan. This flux enhancement could of course suggest that nonthermal processes may play an important role. The nonthermal escape of nitrogen neutrals from this satellite has been extensively studied in previous works. A total loss rate of nonthermal N atoms was estimated to be $<10^{25}$ s^{-1} on the basis of Voyager/UVS observations of airglow emissions [*Strobel et al.*, 1992], consistent with the more recent value of 8.3×10^{24} s^{-1} based on Cassini/INMS observations [*De La Haye et al.*, 2007]. The production of suprathermal nitrogen neutrals might be contributed by collisional dissociation and dissociative ionization, atmospheric sputtering by magnetospheric ions and pickup ions, as well as photochemical processes [e.g., *Lammer and Bauer*, 1993; *Cravens et al.*, 1997; *Shematovich et al.*, 2001, 2003; *Michael et al.*, 2005]. Nonthermal escape also dominates over thermal escape for most other planetary atmospheres in the solar system. However, because of the rapid thermal escape of H_2 on Titan, it has long been proposed that nonthermal escape of H_2 is not important

for this satellite [*Hunten*, 1973; *Bertaux and Kockarts*, 1983].

5.1. Saturn's Gravitational Influence

[41] The escape of H_2 on Titan is complicated by the potential influence of Saturn's gravity. *McDonough and Brice* [1973] first proposed the possibility that particles escaping from Titan may be captured by Saturn's strong gravitational field and form into a toroidal cloud near Titan's orbit [see also *Smyth*, 1981; *Hilton and Hunten*, 1988]. Here, we investigate to what extent the escape of H_2 on Titan can be influenced by Saturn's gravity.

[42] As Saturn's gravity is taken into account, all H_2 molecules with trajectories reaching above the Hill sphere (roughly at 20 Titan radii) are able to escape from the satellite, since these particles would be progressively perturbed by Saturn's gravity and eventually end up orbiting with either the planet or the satellite. This implies that the actual H_2 flux at the Hill sphere should include both upward ballistic flow and escaping flow.

[43] To estimate this effect, a Monte Carlo simulation is performed to numerically integrate the trajectories of test particles in a collisionless exosphere. The test particles start the simulation at the altitude of Titan's exobase with a velocity vector randomly selected from the upward flux of a Maxwellian distribution with a temperature of 152.5 K [*Brinkmann*, 1970]. The trajectories of the test particles are then integrated forward with an adaptive step-sized Bulirsch-Stoer routine according to the equations of motion for the circular restricted three-body problem, with Titan and Saturn treated as the perturbing bodies. The particles are followed until they either return to the exobase or reach the outer boundary of the simulation with a kinetic energy greater than Titan's gravitational potential. The H_2 density profile above Titan's exobase calculated from the Monte Carlo simulation is shown as the dotted line in Figure 3. Its difference with the traditional collisionless model calculated with the same exobase temperature (given by the solid line), is completely due to the inclusion of Saturn's gravitational influence. The H_2 flux is calculated in spherical bins over Titan using the trajectories of one million test particles. We find that Saturn's gravitational influence causes the flux in the simulation to be 23% higher than the Jeans value. This demonstrates that Saturn's gravity is only responsible for a small fraction of the enhanced escape of H_2 on Titan.

5.2. Effect of Diffusive Motion

[44] The conventional way to calculate the thermal escape flux on planetary atmospheres is to use the Jeans formula, which is based on an integration of the Maxwellian distribution for all escaping particles. A preliminary correction to the Jeans flux can be obtained by noting that the nonzero escape flux is naturally associated with the bulk diffusive motion for the escaping component [e.g., *Chamberlain and Campbell*, 1967]. Therefore the VDF at Titan's exobase should be taken as a drifting Maxwellian distribution, with the form

$$f_5 = n_{\text{exo}}\left(\frac{m}{2\pi kT}\right)^{3/2} \exp\left(-\frac{mc^2}{2kT}\right), \tag{17}$$

where $\vec{c} = \vec{v} - \vec{u}$ is the random velocity with $\vec{u}$ being the drift velocity. The subscript "5" is used to emphasize that the drifting Maxwellian is essentially the 5-moment approximation to the full kinetic model, as compared with the 13-moment approximation introduced in section 4.1.

[45] We integrate equation (17) over all escaping particles at the exobase, with a temperature of 152.5 K and a drift velocity of 1.3×10^4 cm s^{-1} from the diffusion model. This gives an H_2 flux of 6.2×10^9 cm^{-2} s^{-1}, more than a factor of 2 smaller than the value derived from the diffusion model. Therefore taking into account the bulk motion does not help to interpret the required flux enhancement.

5.3. Non-Maxwellian Feature of the Velocity Distribution Function

[46] A useful technique for obtaining approximate expressions for the VDF is to choose the drifting Maxwellian distribution as the zeroth-order function and expanding the real VDF in a complete orthogonal series [*Schunk and Nagy*, 2000]. In the 13-moment approximation, the expansion is truncated to include velocity moments up to the heat flux vector and stress tensor. Such a truncated series expansion has the form

$$\frac{f_{13}}{f_5} = 1 - \frac{m\eta}{kTp}\left(\frac{du}{dr} - \frac{u}{r}\right)\left(c_r^2 - \frac{c^2}{3}\right) + \left(1 - \frac{mc^2}{5kT}\right)\frac{m\kappa}{kTp}\frac{dT}{dr}c_{\rm r}, \tag{18}$$

where p is the partial pressure of H_2, $c_{\rm r}$ is the radial component of the random velocity, and other quantities have been defined in equations (3), (4) and (17). The last two terms on the right-hand side of equation (18) represent contributions from viscosity and thermal conduction, respectively.

[47] Thermal escape flux can be obtained by integrating equation (18) over all particles with kinetic energy exceeding the gravitational potential. An inherent assumption in this procedure is that the region above the level for performing such an integration is completely collision-free, therefore any particle injected from that level with $v > v_{\rm esc}$ is able to escape without a further collision to alter its trajectory. The lowest choice of this level can be estimated as $\sim$1600 km from the vertical variation of energy flux shown in Figure 6. Here we apply equation (18) to a range of altitudes between 1600 and 2500 km, with all physical parameters such as temperature and heat flux adopted from the 13-moment calculations in section 4.1. The mean thermal escape flux calculated at these levels is 1.1×10^{10} cm^{-2} s^{-1} referred to Titan's surface, with a variation of $\sim$20% depending on the exact altitude where the integration over equation (18) is performed.

[48] The 13-moment approximation provides a further correction to the thermal escape flux calculated from either the widely used Jeans formula or the drifting Maxwellian distribution. The H_2 flux calculated in such an approximation is a factor of 2.4 higher than the Jeans value. Considering the minor enhancement due to Saturn's gravity (see section 5.1), we suggest that the large H_2 flux of 1.4×10^{10} cm^{-2} s^{-1} on Titan, as inferred from the diffusion model, can be interpreted by thermal escape alone, and nonthermal processes are not required.

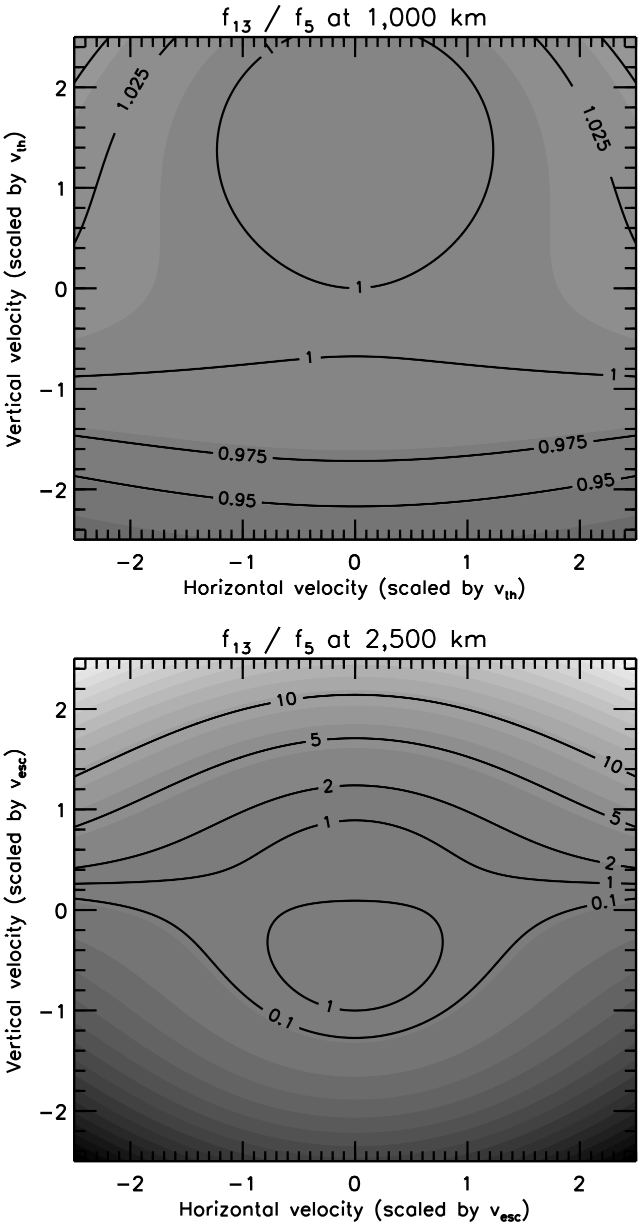

Figure 8. The full two-dimensional velocity distribution in the 13-moment approximation (scaled by the drifting Maxwellian), plotted as a function of horizontal and radial velocities (scaled by either the local thermal velocity or the local escape velocity). Several representative contours are drawn. The velocity distribution at (top) 1000 km and (bottom) 2500 km are shown. Departure from Maxwellian is clearly seen at high altitudes.

[49] The correction to the Jeans flux based on the 13-moment approximation comes primarily from the effect of thermal conduction. To investigate the contribution of thermal conduction alone, we run our 13-moment model with the viscosity term ignored in both equations (3) and (18). This gives a similar thermal structure of H_2 and an H_2 escape flux very close to the value obtained in the full 13-moment approximation.

[50] In Figure 8 we show the 13-moment VDF calculated from equation (18) (normalized by the drifting Maxwellian), as a function of vertical and horizontal velocities (scaled by either the local thermal velocity or the local escape velocity). The upper panel represents the VDF at the lower boundary of 1000 km, which shows that the velocity distribution of H_2 molecules is close to Maxwellian, representing a situation with near thermal equilibrium between H_2 and N_2. With increasing altitude, the deviation from the Maxwellian VDF becomes significant, which is clearly seen in Figure 8 (bottom), calculated at our upper boundary of 2500 km. Several features can be identified from Figure 8:

[51] 1. Compared with the drifting Maxwellian, the 13-moment VDF presents a depletion of particles with $v < -v_{esc}$, corresponding to an absence of incoming hyperbolic particles. This is expected for any exospheric model since the collision frequency at such high altitudes is too low to allow a steady population of incoming hyperbolic particles to be established.

[52] 2. The 13-moment VDF shows an enhanced population of particles with $v > v_{esc}$, especially along the radial direction. These particles are expected to carry the conductive heat flux required by the local energy budget. Figure 9 gives the velocity distribution (scaled by the drifting Maxwellian) in the radial direction at the upper boundary of 2500 km, which shows the depletion of slow particles as well as the accumulation of fast particles more explicitly.

[53] The implications of the results presented here deserve some further concern. First, we notice that the continuity of escape flux is satisfied exactly in the traditional Jeans formalism, since the upward and downward ballistic flows are in perfect balance, with the integration over escaping particles alone giving the accurate total flux. However, this is not exactly true in the 13-moment approximation. The values of the thermal escape flux derived at

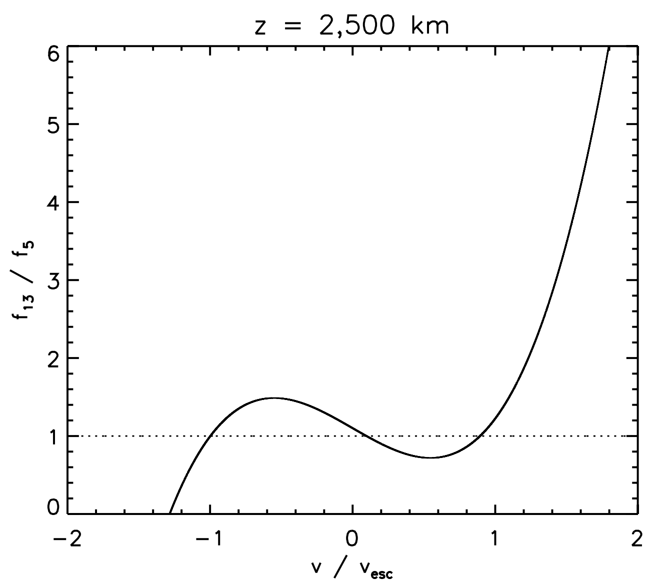

Figure 9. The one-dimensional velocity distribution in the 13-moment approximation (scaled by the drifting Maxwellian), plotted as a function of the radial velocity (scaled by the local escape velocity). Horizontal velocities are taken to be zero for simplicity and a reference altitude of 2500 km is adopted, corresponding to the upper boundary in the 13-moment model.

different altitudes (between 1600 km and 2500 km) but all referred to the surface show some variation at about 20% level, implying that the continuity of escape flux is not perfectly satisfied. More specifically, the integration over all escaping particles gives an estimate of the thermal escape flux of $\sim 9 \times 10^9$ cm^{-2} s^{-1} at 1600 km and $\sim 1.3 \times 10^{10}$ cm^{-2} s^{-1} at 2500 km, where both flux values are referred to the surface. Such a feature of imperfect continuity of escape flux might be related to the collisional nature of the 13-moment model, which allows transitions between ballistic and escaping particles in the exosphere in response to rare collisions. In such a model, the perfect balance between upward and downward ballistic flows is clearly not ensured, and the integration over escaping particles gives a representation of the thermal loss rate, rather than an exact physical value.

[54] Second, the traditional exobase level is placed at 1400–1500 km for Titan, based on a comparison between the local scale height and mean free path. Here an inherent assumption is that all gas components are stationary. However, the H_2 gas is escaping with a considerable drift velocity, which contributes to an additional collisional term in the energy equation (the second term on the right-hand side of equation (3)). This term, representing the deceleration of bulk motion by molecular diffusion, helps to raise the actual exobase level by several hundreds km. We notice that with this term ignored, the total energy flux shows vanishing divergence at $\sim$1450 km, consistent with the traditional choice of the exobase height. The choice of the exobase level has important effects on the derived thermal escape rate. In fact, when integrating equation (18) over all escaping particles at an altitude of 1500 km, we obtain a flux value about 17% higher than the Jeans value. However, the flux calculated at this altitude does not necessarily mean any realistic physical flux, since the effect of neutral collisions is not negligible as we emphasized above. At higher altitudes where collisions can be safely ignored and the procedure of integrating the VDF over all escaping particles is justified, the perturbation of the VDF by thermal conduction becomes strong enough to raise the thermal escape flux significantly above the Jeans value.

[55] Finally, we notice that in the traditional collisionless model, calculating the thermal escape flux at altitudes above the exobase relies on the integration of the Maxwellian VDF over a truncated region of the momentum space, to include only escaping particles that intersect the exobase. In fact, it is through this procedure of truncation that the continuity of escape flux in the traditional Jeans formalism is naturally satisfied. However, such a truncation is not necessary in the 13-moment model, since escaping particles reaching any level above the exobase may come from all directions as a result of rare collisions in the exosphere. The 13-moment VDF that smoothly occupies the entire momentum space is a more realistic representation of the actual velocity distribution, as compared with the truncated Maxwellian in the collisionless model.

[56] It has been suggested in previous works that a realistic VDF at the exobase shows signatures of particle depletion on the high-velocity tail of the Maxwellian distribution as a result of thermal escape [*Fahr and Shizgal*, 1983, and references therein]. This effect tends to reduce the thermal escape rate, contrary to the result presented here. However, the earlier works neglected the effects of thermal conduction that we show to be of paramount importance. Further investigations including application of the 13-moment equation to escape from other planetary atmospheres are needed to understand the full implications of our results. Despite this, we notice that earlier Monte Carlo simulations [e.g., *Chamberlain and Campbell*, 1967; *Brinkmann*, 1970] share the common procedure of picking random source particles from an assumed Maxwellian VDF at the lower boundary (either drifting or nondrifting). However, Figure 6 shows that the heat flux tends to a finite value of 1.6×10^{-4} ergs cm^{-2} s^{-1} near an altitude of 1000 km, which implies the presence of the non-Maxwellian VDF well below the exobase. To assess the importance of this effect, we examined the solution to equation (3) by adopting a heat flux at the lower boundary equal to half of the value satisfying energy continuity. This gives a thermal escape flux in the 13-moment approximation $\sim$30% lower than the Jeans value. By comparison, with the boundary condition satisfying energy continuity, the 13-moment flux is higher by a factor of $\sim$2.5. This suggests that the reduced thermal escape rate claimed in earlier works is probably associated with the (incorrect) neglect of thermal conduction well below the exobase.

6. Discussions and Conclusions

[57] We extract the average H_2 density profile at altitudes between 1000 and 6000 km for Titan's thermosphere and exosphere by combining the INMS measurements from 14 low-altitude encounters of Cassini with Titan. The average N_2 distribution, obtained from the same sample, suggests a temperature of 152.5 K, consistent with previous results [e.g., *Vervack et al.*, 2004].

[58] Below the exobase, the observed H_2 distribution is well described by the diffusion model, with a most probable H_2 flux of 1.37×10^{10} cm^{-2} s^{-1}, referred to the surface. The model assumes full thermal equilibrium between H_2 and N_2. Above Titan's exobase, the H_2 density profile can be described by a simple collisionless model, including both ballistic and escaping molecules. The collisionless model assumes a Maxwellian VDF for H_2 at the exobase, with a most probable exobase temperature of 151.2 K. Interactions with solar EUV photons and energetic particles in Saturn's magnetosphere have negligible effects on the exospheric distribution of H_2 on Titan.

6.1. Thermal Effect

[59] By assuming continuity of energy flux at the upper boundary of 2500 km, we obtain a numerical solution to the H_2 thermal structure for Titan's upper atmosphere, which presents a small temperature decrement of $\sim$2 K between 1000 and 2500 km. This is a result of the local energy budget in Titan's upper thermosphere, in which thermal conduction plays an essential role and naturally accounts for the temperature decrement for H_2. The energy budget implied in the 13-moment approximation is more thorough and complicated than that suggested in early works for the terrestrial exosphere [e.g., *Fahr*, 1976]. The variation of the total H_2 energy flux suggests an exobase level of $\sim$1600 km, which is significantly higher than the traditional

Table 3. Thermal Escape of H_2 on Titan

F_s[a] (cm^{-2} s^{-1})	R[b] (s^{-1})	Note
1.4×10^{10}	1.2×10^{28}	inferred from data
4.5×10^{9}	3.8×10^{27}	Jeans escape
5.4×10^{9}	4.5×10^{27}	Jeans escape including Saturn's gravity
6.2×10^{9}	5.2×10^{27}	drifting Maxwellian
1.1×10^{10}	9.2×10^{27}	13-moment

[a]F_s denotes the H_2 escape flux, referred to Titan's surface.
[b]R denotes the H_2 escape rate, equal to the escape flux multiplied by Titan's surface area.

choice of 1400–1500 km, as a result of the deceleration of the H_2 bulk motion by molecular diffusion through N_2.

6.2. Enhanced Escape

[60] The orthogonal series expansion in the 13-moment approximation defines a non-Maxwellian VDF that includes the effects of both thermal conduction and viscosity (see equation (18)). Integrating over such a VDF for all escaping particles at a range of altitudes above the exobase gives a mean H_2 flux of 1.1×10^{10} cm^{-2} s^{-1} referred to the surface, with an uncertainty of ~20% associated with the exact altitude level (between 1600 and 2500 km) where the integration is performed. Below 1600 km, the effect of collisions between H_2 and N_2 cannot be ignored, and the integration of the VDF over all escaping particles to estimate the thermal escape flux is not justified. The escape flux implied by the 13-moment model is significantly higher than the Jeans value and roughly matches the flux inferred from the diffusion equation. The 13-moment model interprets the enhanced escape as a result of the accumulation of H_2 molecules on the high-energy portion of the VDF, primarily associated with the conductive heat flux. In this work, the enhanced escape of H_2 on Titan is still thermal in nature. Nonthermal processes are not required to interpret the loss of H_2 on Titan.

[61] In a recent work by *Strobel* [2008], the thermal escape process on Titan was investigated by solving the hydrodynamic equations for a single component N_2 atmosphere, which gave a hydrodynamic escape rate of 4.5×10^{28} amu s^{-1} (the sum of H_2 and CH_4 escape), restricted by power limitations. Assuming that the ratio between individual loss rates is equal to the corresponding limiting flux ratio, *Strobel* [2008] obtained an H_2 loss rate of 5.3×10^{27} s^{-1}, or an H_2 flux of 6.3×10^{9} cm^{-2} s^{-1}, referred to Titan's surface. This indicates that by treating the thermal escape process as hydrodynamic rather than stationary (as implicitly assumed in the Jeans formula), the derived H_2 escape rate exceeds the Jeans value by ~40%, to be compared with the 13-moment calculation of the flux enhancement of about a factor of 3.

[62] The approach followed by *Strobel* [2008] is quite different from that adopted here, in the sense that he assumed constant composition and worked entirely in the fluid, rather than the kinetic regime. Escape in Strobel's model is due entirely to bulk outflow of the atmosphere whereas in our calculations escape is driven primarily by the perturbations to the VDF due to the heat flow. Instead, the primarily effect of bulk outflow is to raise the exobase to a higher level at ~1600 km, where the perturbation of the VDF by thermal conduction becomes strong enough to have an appreciate effect on the thermal escape rate. In terms of perturbations to the VDF, the heat flow is more important than the drift velocity. On the other hand, *Strobel* [2008] did carefully treat the energy balance in the upper thermosphere and argued that it is the energetics that causes the large loss rates and the breakdown of Jeans escape. In that sense, his results are consistent with those found here in terms of the importance of energy continuity to the molecular escape rate. The characters of Strobel's fluid solutions are determined by requiring energy continuity and that the energy escape flux be consistent with the mass escape flux. These requirements coupled with the Navier-Stokes equations imply an escape rate significantly greater than Jeans escape. The same requirement on consistency between mass and energy escape also appears in our calculations, in which the boundary condition on the energy flux forces a negative temperature gradient. The associated heat flux alters the VDF and thereby enhances the escape rate in the kinetic description. It is worth restating that one of the fundamental assumptions in Jeans escape is that the atmospheric energetics is unaffected by escape. In both Strobel's approach and ours, it is the effect of the escape process on the atmospheric energetics that causes the high escape rates and the failure of Jeans escape. What is most surprising is that Jeans escape fails for such small values of the energy flux. An energy flux corresponding to a temperature drop across the transition region of several kelvin causes more than a factor of 2 increase in the escape flux. It appears important to determine under what conditions the Jeans escape formula can reliably be used.

[63] Finally, we summarize all the relevant fluxes in Table 3, in which F_s is the thermal escape fluxes calculated in various ways (all referred to Titan's surface) and R is the corresponding escape rates. A complete interpretation of the enhanced escape has to rely on a proper consideration of both bulk outflow and thermal conduction. The former controls the exact level of the exobase, while the latter drives significant departures from the Maxwellian so that the actual thermal escape rate is significantly higher than the Jeans value. In a more general context, enhanced escape induced by bulk outflow and thermal conduction is expected to be a common feature for planetary atmospheres. The 13-moment kinetic model presented in this paper will be applied to other planetary systems in follow-up studies.

Appendix A: Energy Density and Flux in the 13-Moment Approximation

[64] In the 13-moment approximation, the continuity, momentum and energy equations for a diffusing neutral component can be expressed as

$$\frac{\partial n}{\partial t} + \frac{\partial}{\partial x_i}(nu_i) = 0, \tag{A1}$$

$$mn\left(\frac{\partial u_i}{\partial t} + u_j\frac{\partial u_i}{\partial x_j}\right) + \frac{\partial p}{\partial x_i} + \frac{\partial \tau_{ji}}{\partial x_j} - mng_i = \frac{\delta M_i}{\delta t}, \tag{A2}$$

$$\frac{3}{2}\frac{\partial p}{\partial t} + \frac{3}{2}u_i\frac{\partial p}{\partial x_i} + \frac{5}{2}p\frac{\partial u_i}{\partial x_i} + \frac{\partial q_i}{\partial x_i} + \tau_{ij}\frac{\partial u_i}{\partial x_j} = \frac{\delta E}{\delta t}, \tag{A3}$$

where n, p, u_i, q_i, τ_{ij} are the density, pressure, drift velocity vector, heat flux vector and stress tensor of the neutral species, with i, j = 1, 2, 3 characterizing components along the three orthogonal spatial coordinates (x_i), and $\delta M_i/\delta t$ and $\delta E/\delta t$ are the momentum and energy integrals [*Schunk and Nagy*, 2000]. Here, for repeated indices, the Einstein summation convention is assumed. Equation (A3) can be recast as

$$\frac{3}{2}\frac{\partial p}{\partial t}+\frac{5}{2}\frac{\partial}{\partial x_i}(pu_i)-u_i\frac{\partial p}{\partial x_i}+\frac{\partial q_i}{\partial x_i}+\tau_{ij}\frac{\partial u_i}{\partial x_j}=\frac{\delta E}{\delta t}. \quad \text{(A4)}$$

Using equation (A2) to eliminate $u_i\partial p/\partial x_i$, we get

$$\frac{3}{2}\frac{\partial p}{\partial t}+\frac{5}{2}\frac{\partial}{\partial x_i}(pu_i)+mn\frac{\partial}{\partial t}\left(\frac{1}{2}u^2\right)+mnu_iu_j\frac{\partial u_i}{\partial x_j}+u_i\frac{\partial \tau_{ji}}{\partial x_j} - mnu_ig_i+\frac{\partial q_i}{\partial x_i}+\tau_{ij}\frac{\partial u_i}{\partial x_j}=\frac{\delta E}{\delta t}+u_i\frac{\delta M_i}{\delta t}, \quad \text{(A5)}$$

where $u^2 = u_iu_i$. The gravity term in equation (A5) can be expressed as

$$\begin{aligned} -mnu_ig_i &= -mnu_i\frac{\partial}{\partial x_i}\left(\frac{GM}{r}\right) \\ &= -\frac{\partial}{\partial x_i}\left(\frac{GMm}{r}nu_i\right)+\frac{GMm}{r}\frac{\partial}{\partial x_i}(nu_i) \\ &= -\frac{\partial}{\partial x_i}\left(\frac{GMm}{r}nu_i\right)-\frac{GMm}{r}\frac{\partial n}{\partial t}, \end{aligned} \quad \text{(A6)}$$

where $r = (x_ix_i)^{1/2}$, M is the planet mass, G is the gravitational constant, and we have used equation (A1) to eliminate $\partial(nu_i)/\partial x_i$ in the last equality. The term, $mnu_iu_j(\partial u_i/\partial x_j)$ in equation (A5) can be recast as

$$mnu_iu_j\frac{\partial u_i}{\partial x_j}=\frac{\partial}{\partial x_j}\left(mnu^2u_j\right)-u^2\frac{\partial}{\partial x_j}\left(mnu_j\right)-mnu_iu_j\frac{\partial u_i}{\partial x_j}, \quad \text{(A7)}$$

which gives

$$\begin{aligned} mnu_iu_j\frac{\partial u_i}{\partial x_j} &= \frac{\partial}{\partial x_j}\left(\frac{1}{2}mnu^2u_j\right)-\frac{1}{2}u^2\frac{\partial}{\partial x_j}\left(mnu_j\right) \\ &= \frac{\partial}{\partial x_j}\left(\frac{1}{2}mnu^2u_j\right)+\frac{1}{2}mu^2\frac{\partial n}{\partial t}. \end{aligned} \quad \text{(A8)}$$

Finally, we write $u_i(\partial\tau_{ji}/\partial x_j)$ as

$$u_i\frac{\partial \tau_{ji}}{\partial x_j}=\frac{\partial}{\partial x_j}\left(u_i\tau_{ji}\right)-\tau_{ji}\frac{\partial u_i}{\partial x_j}. \quad \text{(A9)}$$

Using equations (A6), (A8), and (A9), equation (A5) can be expressed as

$$\frac{\delta E}{\delta t}+u_i\frac{\delta M_i}{\delta t}=\frac{\partial}{\partial t}\left(\frac{3}{2}p+\frac{1}{2}mnu^2-\frac{GMm}{r}n\right)+\frac{\partial}{\partial x_j}\left(\frac{5}{2}pu_j+\frac{1}{2}mnu^2u_j+u_i\tau_{ji}-\frac{GMm}{r}nu_j+q_j\right), \quad \text{(A10)}$$

where we have used the fact that τ_{ij} is symmetric.

[65] We further recast equation (A10) as

$$\frac{\partial \epsilon}{\partial t}+\frac{\partial}{\partial x_j}\left(\phi_j+u_i\tau_{ji}+q_j\right)=\frac{\delta E}{\delta t}+u_i\frac{\delta M_i}{\delta t}. \quad \text{(A11)}$$

Clearly, ϵ and ϕ_j represent the energy density and energy flux, with the definitions of

$$\epsilon = mn\left(c_vT+\frac{1}{2}u^2-\frac{GM}{r}\right), \quad \text{(A12)}$$

$$\phi_j = mnu_j\left(c_pT+\frac{1}{2}u^2-\frac{GM}{r}\right), \quad \text{(A13)}$$

where we have replaced p by nkT with k being the Boltzmann constant and T being the gas temperature, c_v = (3/2)(k/m) and c_p = (5/2)(k/m) are the specific heat capacities at constant volume and pressure. The terms, $u_i\tau_{ji}$ and q_j in equation (A11) represent energy fluxes associated with viscous dissipation and thermal conduction, respectively. Assuming spherical symmetry, we can express the radial components of these energy fluxes as

$$(q_i)_r = -\kappa\frac{dT}{dr}, \quad \text{(A14)}$$

$$(u_i\tau_{ji})_r = -\frac{4}{3}\eta u\left(\frac{du}{dr}-\frac{u}{r}\right), \quad \text{(A15)}$$

where κ is the thermal conductivity and η is the viscosity coefficient.

[66] **Acknowledgments.** We are grateful to D. F. Strobel, I. C. F. Müller-Wodarg, D. M. Hunten, and R. Malhotra for helpful discussions. This work is supported by NASA through grant NAG5-12699 to the Lunar and Planetary Laboratory, University of Arizona.

References

Abgrall, H., J. Le Bourlot, G. Pineau Des Forets, E. Roueff, D. R. Flower, and L. Heck (1992), Photodissociation of H_2 and the H/H_2 transition in interstellar clouds, *Astron. Astrophys.*, *253*, 525–536.

Abgrall, H., E. Roueff, and I. Drira (2000), Total transition probability and spontaneous radiative dissociation of B, C, B′ and D states of molecular hydrogen, *Astron. Astrophys. Suppl.*, *141*, 297–300.

Atreya, S. K., P. B. Hays, and A. F. Nagy (1975), Doppler profile measurements of the geocoronal hydrogen Balmer alpha line, *J. Geophys. Res.*, *80*, 635–638.

Bertaux, J. L., and G. Kockarts (1983), Distribution of molecular hydrogen in the atmosphere of Titan, *J. Geophys. Res.*, *88*, 8716–8720.

Boqueho, V., and P.-L. Blelly (2005), Contributions of a multimoment multispecies approach in modeling planetary atmospheres: Example of Mars, *J. Geophys. Res.*, *110*, A01313, doi:10.1029/2004JA010414.

Brinkmann, R. T. (1970), Departures from Jeans' escape rate for H and He in the Earth's atmosphere, *Planet. Space Sci.*, *18*, 449–478.

Chamberlain, J. W. (1963), Planetary coronae and atmospheric evaporation, *Planet. Space Sci.*, *11*, 901–960.

Chamberlain, J. W., and F. J. Campbell (1967), Rate of evaporation of a non-Maxwellian atmosphere, *Astrophys. J.*, *149*, 687–705.

Chamberlain, J. W., and D. M. Hunten (1987), *Theory of Planetary Atmospheres: An Introduction to Their Physics and Chemistry, Int. Geophys. Ser.*, vol. 36, edited by W. L. Donn, pp. 335–340, Academic, San Diego, Calif.

Chapman, S., and T. G. Cowling (1970), *The Mathematical Theory of Non-uniform Gases*, 3rd ed., Cambridge Univ. Press, Cambridge, U.K.

Cravens, T. E., C. N. Keller, and B. Ray (1997), Photochemical sources of non-thermal neutrals for the exosphere of Titan, *Planet. Space Sci.*, *45*, 889–896.

De La Haye, V., et al. (2007), Cassini Ion and Neutral Mass Spectrometer data in Titan's upper atmosphere and exosphere: Observation of a suprathermal corona, *J. Geophys. Res.*, *112*, A07309, doi:10.1029/2006JA012222.

Fahr, H. J. (1976), Reduced hydrogen temperatures in the transition region between thermosphere and exosphere, *Ann. Geophys.*, *32*, 277–282.

Fahr, H. J., and B. Shizgal (1983), Modern exospheric theories and their observational relevance, *Rev. Geophys.*, *21*, 75–124.

Fahr, H. J., and B. Weidner (1977), Gas evaporation from collision-determined planetary exospheres, *Mon. Not. R. Astron. Soc.*, *180*, 593–612.

Hilton, D. A., and D. M. Hunten (1988), A partially collisional model of the Titan hydrogen torus, *Icarus*, *73*, 248–268.

Hunten, D. M. (1973), The escape of H_2 from Titan, *J. Atmos. Sci.*, *30*, 726–732.

Kim, Y. K., and M. E. Rudd (1994), Binary-encounter-dipole model for electron-impact ionization, *Phys. Rev. A*, *50*, 3954–3967.

Lammer, H., and S. J. Bauer (1993), Atmospheric mass loss from Titan by sputtering, *Planet. Space Sci.*, *41*, 657–663.

Lebonnois, S., E. L. O. Bakes, and C. P. McKay (2003), Atomic and molecular hydrogen budget in Titan's atmosphere, *Icarus*, *161*, 474–485.

Lemaire, J. F., W. K. Peterson, T. Chang, R. W. Schunk, A. R. Barakat, H. G. Denars, and G. V. Khazanov (2007), History of kinetic polar wind models and early observations, *J. Atmos. Sol. Terr. Phys.*, *69*, 1901.

Mason, E. A., and T. R. Marrero (1970), The diffusion of atoms and molecules, in *Advances in Atomic and Molecular Physics*, edited by D. R. Bates and I. Esterman, pp. 155–232, Academic, San Diego, Calif.

McClure, G. W. (1966), Electron transfer in proton-hydrogen-atom collisions: 2–117 keV, *Phys. Rev.*, *148*, 47–54.

McDonough, T. R., and N. M. Brice (1973), New kind of ring around Saturn, *Nature*, *242*, 513.

Michael, M., R. E. Johnson, F. Leblanc, M. Liu, J. G. Luhmann, and V. I. Shematovich (2005), Ejection of nitrogen from Titan's atmosphere by magnetospheric ions and pick-up ions, *Icarus*, *175*, 263–267.

Müller-Wodarg, I. C. F., R. V. Yelle, J. Cui, and J. H. Waite (2008), Horizontal structures and dynamics of Titan's thermosphere, *J. Geophys. Res.*, *113*, E10005, doi:10.1029/2007JE003033.

Nutt, W. L., R. W. McCullough, and H. B. Gilbody (1979), Electron capture by 04–13 keV C^+, N^+ and O^+ ions in H and H_2, *J. Phys. B At. Molec. Phys.*, *12*, L157–L161.

Öpik, E. J., and S. F. Singer (1961), A study of hydrogen diffusion in the Earth's upper atmosphere near the critical level, *Phys. Fluids*, *4*, 221–233.

Richardson, J. D. (1995), An extended plasma model for Saturn, *Geophys. Res. Lett.*, *22*, 1177–1180.

Richardson, J. D., and E. C. Sittler Jr. (1990), A plasma density model for Saturn based on Voyager observations, *J. Geophys. Res.*, *95*, 12,019–12,031.

Rowley, R. L., W. V. Wilding, J. L. Oscarson, and Y. Yang (2003), *Physical and Thermodynamic Properties of Pure Chemicals*, Core Edition Plus Supplements 1–13, Taylor and Francis, New York.

Schunk, R. W., and A. F. Nagy (2000), *Ionospheres: Physics, Plasma Physics, and Chemistry*, edited by A. J. Dressler, J. T. Houghton, and M. J. Rycroft, pp. 52–100, Cambridge Univ. Press, Cambridge, U.K.

Shematovich, V. I., C. Tully, and R. E. Johnson (2001), Suprathermal nitrogen atoms and molecules in Titan's corona, *Adv. Space Res.*, *27*, 1875–1880.

Shematovich, V. I., R. E. Johnson, M. Michael, and J. G. Luhmann (2003), Nitrogen loss from Titan, *J. Geophys. Res.*, *108*(E8), 5087, doi:10.1029/2003JE002094.

Sittler, E. C., Jr., K. W. Ogilvie, and J. D. Scudder (1983), Survey of low-energy plasma electrons in Saturn's magnetosphere: Voyagers 1 and 2, *J. Geophys. Res.*, *88*, 8847–8870.

Smyth, W. H. (1981), Titan's hydrogen torus, *Astrophys. J.*, *246*, 344–353.

Strobel, D. F. (2008), Titan's hydrodynamically escaping atmosphere, *Icarus*, *193*, 588–594.

Strobel, D. F., M. E. Summers, and X. Zhu (1992), Titan's upper atmosphere - structure and ultraviolet emissions, *Icarus*, *100*, 512–526.

Tam, S. W. Y., T. Chang, and V. Pierrard (2007), Kinetic modeling of the polar wind, *J. Atmos. Sol. Terr. Phys.*, *69*, 1984–2027, doi:10.1016/j.jastp.2007.08.006.

Vervack, R. J., B. R. Sandel, and D. F. Strobel (2004), New perspectives on Titan's upper atmosphere from a reanalysis of the Voyager I UVS solar occultations, *Icarus*, *170*, 91–112.

Vuitton, V., R. V. Yelle, and J. Cui (2008), Formation and distribution of benzene on Titan, *J. Geophys. Res.*, *113*, E05007, doi:10.1029/2007JE002997.

Waite, J. H., Jr., et al. (2004), The Cassini Ion and Neutral Mass Spectrometer (INMS) investigation, *Space Sci. Rev.*, *114*, 113–231.

Wilson, E. H., and S. K. Atreya (2004), Current state of modeling the photochemistry of Titan's mutually dependent atmosphere and ionosphere, *J. Geophys. Res.*, *109*, E06002, doi:10.1029/2003JE002181.

Woods, T. N., G. J. Rottman, S. M. Bailey, S. C. Solomon, and J. R. Worden (1998), Solar extreme ultraviolet irradiance measurements during solar cycle 22, *Sol. Phys.*, *177*, 133–146.

Yan, M., H. R. Sadeghpour, and A. Dalgarno (1998), Photoionization cross sections of He and H_2, *Astrophys. J.*, *496*, 1044–1050.

Yelle, R. V., N. Borggren, V. De La Haye, W. T. Kasprzak, H. B. Niemann, I. C. F. Müller-Wodarg, and J. H. Waite Jr. (2006), The vertical structure of Titan's upper atmosphere from Cassini Ion Neutral Mass Spectrometer measurements, *Icarus*, *182*, 567–576.

Yelle, R. V., J. Cui, and I. C. F. Müller-Wodarg (2008), Methane escape from Titan's atmosphere, *J. Geophys. Res.*, *113*, E10003, doi:10.1029/2007JE003031.

J. Cui, K. Volk, and R. V. Yelle, Lunar and Planetary Laboratory, University of Arizona, 1629 E. University Boulevard, Tucson, AZ 85721, USA. (jcui@lpl.arizona.edu)